DR. NIKOLAUS BERNDT (Orcid ID : 0000-0001-5594-9940)

MRS. MADLEN MATZ-SOJA (Orcid ID : 0000-0002-5929-3704)

Article type : Original

Manuscript identification number HEP-19-1360

Functional consequences of metabolic zonation in murine livers: New insights for an old story

Nikolaus Berndt[1#], Erik Kolbe[2#], Robert Gajowski[3,4], Johannes Eckstein[5], Fritzi Ott[2], David Meierhofer[3], Hermann Georg Holzhütter[5+], Madlen Matz-Soja[2, 6+]

[1] Charité – Universitätsmedizin Berlin, corporate member of Freie Universität Berlin, Humboldt-Universität zu Berlin, and Berlin Institute of Health, Institute for Computational and Imaging Science in Cardiovascular Medicine, Berlin, Germany

[2] Rudolf-Schönheimer-Institute of Biochemistry, Faculty of Medicine, Leipzig University Leipzig, Germany

[3] Max Planck Institute for Molecular Genetics, Berlin, Germany

[4] Fachbereich Biologie, Chemie, Pharmazie, Freie Universität Berlin, Germany

[5] Charité – Universitätsmedizin Berlin, corporate member of Freie Universität Berlin, Humboldt-Universität zu Berlin, and Berlin Institute of Health, Institute of Biochemistry, Berlin, Germany

[6] University Clinic Leipzig, Clinic and Polyclinic for Gastroenterology, Infectiology and Pneumology, Division of Hepatology, Leipzig, Germany

[#]These authors contributed equally as first authors

[+]Co-senior authorship

Email: nikolaus.berndt@charite.de
Erik.Schroeder@medizin.uni-leipzig.de
gajowski@molgen.mpg.de
johannes.Eckstein@charite.de
Fritzi.Ott@medizin.uni-leipzig.de
meierhof@molgen.mpg.de
hermann-georg.holzhuetter@charite.de
madlen.matz@medizin.uni-leipzig.de

Keywords: HEPATOKIN, metabolic zonation, hepatocytes, FACS, periportal, pericentral

Footnote Page:

Contact Information:
Nikolaus Bernd, Institute of Biochemistry, Charité – Universitätsmedizin, Charitéplatz 1, Berlin, Germany, phone: +49 30450528466; fax: +49 30450528937; email: nikolaus.berndt@charite.de

List of Abbreviations:
TAG, triacylglycerol; PPH, periportal hepatocytes; PCH, pericentral hepatocytes; CCl_4, carbon tetrachloride; *Arg1*, Arginase 1; *Gck*, Glucokinase; *Gls2*, Glutaminase 2; *Ldha*, lactate dehydrogenase A chain; *Krt18*, Keratin 18; *Krt8*, Keratin 8; *Gfap*, glial fibrillary acidic protein; *Acta2,* alpha smooth muscle actin 2; *Emr1*, EGF-like module containing, mucin-like, hormone receptor-like sequence 1; *Krt19*, Keratin 19; E-Cad, E-Cadherin; GLUL, Glutamine Synthetase; FSC-A, forward scatter-area; forward scatter-height; SSC, side scatter; TBST, TRIS buffered saline with TWEEN; CPS1, carbamoyl-phosphate synthase 1; CYP1A2, cytochrome P450 1A2; CYP2E1, cytochrome P450 2E1; SDC, sodium deoxycholate; TCEP, tris(2-carboxyethyl)phosphine; CAA, chloroacetamide; AGC, automatic gain control; FDR, false discovery rate; LFQ, label free quantification; GHT, glucose-hormone transfer; HPT, hormone-phosphorylation transfer function; OAT, Ornithine Aminotransferase, Cyp7A1, Cytochrome P450 Family 7 Subfamily A Member 1; SFXN1, Sideroflexin 1; COX7A1, Cytochrome C Oxidase Subunit 7A1; HSD17B6, Hydroxysteroid 17-Beta Dehydrogenase 6; PIGR, Polymeric Immunoglobulin Receptor; LGASL1, Galectin 1; SHROOM,

Shroom Family Member; FFAs, free fatty acids; VLDL, very low density lipoprotein; DNL, *de novo* lipogenesis; GLUT2, glucose transporter 2; PC, pyruvate carboxylase; PEPCK, phospoenolpyruvate carboxylase; FBP2, fructose bisphosphatase 2; PFK2, phosphofructokinase 2; GK, glucokinase; PDHC, pyruvate dehydrogenase; NAD, nikotinamid adenine dinucleotide; ALDH, acetaldehyde dehydrogenase

Financial Support:

This work was supported by the Federal Ministry of Education and Research (Germany) within the research network Systems Medicine of the Liver (LiSyM) [grant number 031L0053, 31L0057, 031L0058] and the Deutsche Forschungsgemeinschaft (Bonn, Germany) [grant MA 6610/2-1, MA6610/4-1].

Abstract

Background & Aims: Zone-dependent differences in the expression of metabolic enzymes along the porto-central axis of the acinus are a long-known feature of liver metabolism. A prominent

example is the preferential localization of the enzyme glutamine synthetase in pericentral hepatocytes, where it converts potentially toxic ammonia to the valuable amino acid glutamine. However, with the exception of a few key regulatory enzymes, a comprehensive and quantitative assessment of zonal differences in the abundance of metabolic enzymes and much more importantly, an estimation of the associated functional differences between portal and central hepatocytes is missing thus far.

Approach & Results: We addressed this problem by establishing a new method for the separation of periportal and pericentral hepatocytes that yields sufficiently pure fractions of both cell populations. Quantitative shotgun proteomics identified hundreds of differentially expressed enzymes in the two cell populations. We used zone-specific proteomics data for scaling of the maximal activities to generate portal and central instantiations of a comprehensive kinetic model of central hepatic metabolism (Hepatokin1).

Conclusion: The model simulations revealed significant portal-to-central differences in almost all metabolic pathways involving carbohydrates, fatty acids, amino acids and detoxification.

Introductory Statement

The liver is the central metabolic organ of higher vertebrates and continuously adapts its metabolic capacities to the actual physiological status of the individual. After a carbohydrate-rich meal, a substantial portion of glucose is taken up by the liver from the plasma and is transiently converted into glycogen and triacylglycerol. Conversely, under fasting conditions, the liver produces glucose by phosphorolysis of glycogen and *de novo* synthesis from amino acids, lactate and glycerol to prevent a potentially life-threatening drop in plasma glucose below 55 mg/dL [1]. Intriguingly, the capacity of hepatocytes to take up or to produce glucose varies with their location within the liver acinus. Hepatocytes close to the portal vein (periportal hepatocytes (PPH)) possess a higher gluconeogenic

capacity than hepatocytes close to the central vein (pericentral hepatocytes (PCH)). Conversely, PCH have a higher glycolytic capacity than PHH. Gradual spatial separation of anabolic (ATP-consuming) gluconeogenesis from catabolic (ATP-generating) glycolysis may represent a principle in tissue metabolism to limit the extent of ATP-wasting futile cycles. Another prominent example of zone-dependent metabolic differences is ammonia detoxification. Ammonia fixation in urea is predominantly located in the PP zone, whereas glutamine synthesis is predominantly located in the PC zone [2,3]

Zonal differences in the proteome of hepatocytes are driven by porto-central gradients of oxygen, metabolites (e.g., glucose), hormones and morphogens such as Wnt, Hedgehog and HNFα [4,5]. The opposing effects of the pancreatic hormones insulin and glucagon on the zonation of glycolytic and glucogenic enzymes have been demonstrated in the earlier pioneering *in vitro* studies of Jungermann [6]. Later, flow bioreactors were used to study the impact of selected regulators of zonation by exposing hepatocytes to controlled concentrations gradients of oxygen, metabolites or xenobiotics [7,8]. Using a tissue model of the liver acinus and taking into account known relationships between the protein translation rate and oxygen, glucose, insulin and glucagon concentrations, we were able to recapitulate the zonation of hepatic glucose metabolism under fasting and feeding conditions [9].

Over several decades, the investigation of differential gene expression along the porto-central axis has been restricted to a few key regulatory enzymes. More recently, the group of Shalev Itzkovitz was successful in quantifying the entire transcriptome of thousands of mouse liver cells together with their lobule coordinates [10]. They found that approximately 50 % of liver genes are significantly zonated, but a comprehensive and quantitative analysis of the functional consequences of this zone-specific enrichment was not provided in this pioneering work. Therefore, we have strived to take one step further by mapping the zone-dependent expression data for metabolic enzymes and membrane transporters onto a mechanistic model of the central hepatic metabolism. Therefore, we isolated hepatocytes from the mouse liver by collagenase perfusion and separated PPH and PCH by immunostaining and subsequent cell sorting. We then used shotgun proteomics to explore the proteome of the purified hepatocytes. Specifically, we used relative protein abundances to scale the maximal activities of enzymes and membrane transporters included in a recently published kinetic model of hepatocyte metabolism [11] to assess the implications of zone-dependent gene expression for a multitude of different metabolic functions. A complete list of all enzymes and transporters considered in the model is given in Table S1.

Experimental Procedures

Isolation of primary mouse hepatocytes

The primary hepatocytes were isolated by collagenase perfusion of the mouse liver as described in [12]. Isolated hepatocytes were cleared of nonparenchymal cells via differential centrifugation [13]. We have demonstrated the purity of our primary hepatocyte isolation via this method elsewhere, where we looked for the expression of typical markers of mature hepatocytes such as *Arg1* (Arginase 1), *Gck* (Glucokinase), *Gls2* (Glutaminase 2 (liver, mitochondrial)), *Ldha* (lactate dehydrogenase A chain), *Krt18* (Keratin 18) and *Krt8* (Keratin 8). For the nonparenchymal cell population (e.g., hepatic stellate cells, vascular smooth muscle cells Kupffer cells and cholangiocytes), we analyzed *Gfap* (glial fibrillary acidic protein), *Acta2* (actin, alpha 2, smooth muscle, aorta), *Emr1* (EGF-like module containing, mucin-like, hormone receptor-like sequence 1), and *Krt19* (Keratin 19) [13].

Other detailed methods are available in the Supporting Information.

Results

Isolation of periportal and pericentral hepatocytes via flow cytometry

To sort the isolated primary hepatocytes into populations of PPH and PCH, specific marker proteins with no overlap in zonal expression (Fig. 2A) were chosen for intracellular staining. After excluding cell doublets in the FSC-A vs. FSC-H plot and cell debris in the FSC vs. SSC plot, the positive cell populations were gated against matching isotype controls (Fig. S1, S2). The relative proportion of positively labeled cells in both stainings reflects the extended PP (periportal) pattern of E-Cadh. in contrast to the small, one-cell-layer PC (pericentral) localization of GLUL, as indicated by immunohistochemistry staining (Fig. S3). E-Cadh. labeling (Fig. S3, left panel) resulted in large populations of approximately 30–50 %, whereas GLUL labeling (Fig. S3, right panel) resulted in small populations of approximately 1.5–3.0 %. To give a global overview about the purity of the sorting method the data from proteome analysis were analyzed with regard to all proteins of the individual cell fractions. The results of this analysis shows that 995 proteins (Table S2, sheet 3 and sheet 4) out of a total of 3736 (Table S3) detected proteins have a significant zonated pattern. A selection of the 40 most potent zonated proteins shows that well known zonated proteins can be

found in both the pericentral and the periportal fraction (Fig 2B; Table 1). Also western blot analysis of PPH and PCH marker proteins demonstrated the purity of the isolation method. Therefore, prominent PC expressed proteins such as GLUL, CYP1A2 and CYP1A2 could not or could only weakly be found in the PPH. The dominant PP expressed protein E-Cadh. could not be detected in the PC fraction. The expression of CPS1 shows stronger expression in the PP zone; however, this protein is also found in the PCH (Fig. 2 C,D). This corresponds to the rather homogeneous distribution of this protein, in which there is a tendency toward expression only in the PP region [14]. In addition Gaasbeek J. and colleagues showed that in the adult rat liver some pericentral hepatocytes habour also carbamoylphosphate synthetase, albeit the number of glutamine synthetase-positive cells diminishes [15].

Differences in the protein abundances of periportal and pericentral hepatocytes

Shotgun proteome profiling yielded protein intensities for 3736 proteins that could be identified in the PPH, the PCH and the reference hepatocytes. Statistical analysis of differences between the protein intensities in the PPH and PCH by means of paired sample *t*-test at a significance level of $p = 0.05$ revealed that 21.9% of the detected proteome was zonated. There were only marginal differences in the percentage of proteins with higher expression levels in either the PPH (13.4%) or the PCH (13.2%).

From the whole detected proteome, we selected 316 proteins that are associated with enzymes and membrane transporters of the kinetic model (i.e., “model proteins”). Within this subgroup, 58.2% of proteins exhibit significant portal-to-central expression differences, which is more than twice as high as in the total proteome. Moreover, a larger fraction of metabolic enzymes has higher protein abundances in PPH (42.7%), while the fraction of metabolic enzymes with higher expression in the PCH was 22.5%. A complete list of differentially expressed proteins can be found in Table S2.

Parameterization of zone-specific kinetic models

To obtain zone-specific instantiations of the metabolic model for each laboratory animal, the maximal activities of enzymes and transporters in the PCH and PPH were computed according to Eq. 1 (see Methods). The average percentage of enzymes and transporters for which a protein intensity value was available from the proteomics analysis was 80.0 %, with the lowest coverage of 64.4 % and the highest coverage of 88.5 %. To fill the gaps, we applied a statistical imputation method that estimates missing values of a given target protein based on the expression profiles of other predictor

proteins with sufficiently similar intensity profiles taken from the same proteome. This method increased the average coverage of measured protein intensity values to 84.1 %, with 77.9 % the lowest coverage and 88.5 % the highest coverage.

First, we compiled a list of potential predictor proteins for which measured protein intensities for the three cell fractions (periportal, pericentral or whole liver) were available for all 6 mice. This resulted in three sets of 1482, 1571 and 1064 predictor proteins. Second, for a given target protein with missing protein intensity values in some mice, we determined a group of significantly Pearson correlated ($p < 0.05$) predictor proteins also exhibiting a Spearman correlation larger than a critical threshold value $\rho > 0.95$. Linear regression analysis with each of these predictor proteins yielded estimates of the missing values. Finally, the missing intensity values were filled by the mean of the estimates obtained for all predictor proteins. For the six mice included in this study, the measured and imputed LFQ intensities for the proteins of the kinetic model are available for the reference cells, the PPH and the PCH in Table S4.

Model-based functional characterization of the PPH and PCH

For the assessment of functional differences between PPH and PCH we used zone-specific kinetic models to compute steady-state load characteristics describing the change of a metabolic function in response to changes in the concentration of a distinct plasma metabolite. Steady-state model computations assume that the characteristic time for the change of the plasma metabolites is much longer than the characteristic time required establishing a stationary state of the metabolic network where the time derivatives of all metabolites are practically zero.

As the cellular metabolic response depends on the extracellular concentrations of insulin, glucagon and all exchangeable external metabolites, we were confronted with a quasi-continuum of external conditions at which load characteristics can be constructed. Therefore, we decided to choose two different types of external conditions. For load characteristics at varying plasma levels of glucose, we used the phenomenological transfer functions GHT and HPT (see Methods) to compute the plasma concentrations of insulin and glucagon from the plasma glucose level and the phosphorylation state of hormone-sensitive interconvertible enzymes. For all other load characteristics, we fixed the external conditions in strict correspondence to the assay conditions applied in the experiments that were used to calibrate the generic kinetic model Hepatokin1. The external conditions for each load characteristic are given in the Table S5.

Zonation of carbohydrate metabolism

The maximal gluconeogenetic capacity of PPH and PCH was analyzed by computing the exchange flux through the glucose transporter at varying concentrations of the precursor metabolite lactate (Fig. 3A). As lactate is converted to pyruvate, this calculation provides a realistic assessment of the gluconeogenetic capacity even under conditions where amino acids serve as the major gluconeogenetic substrate. PPH are predicted to possess a significantly larger gluconeogenic capacity than PCH, and the maximal capacities of the two cell variants differ by more than a factor of two. For both cell types, the half-maximal rate of gluconeogenesis is reached at lactate concentrations of approximately 1 mM, representing the normal physiological plasma value.

Differential capacities of gluconeogenesis and glycolysis in PPH and PCH have a large impact on glucose exchange with the blood. Fig. 3B depicts the glucose exchange flux as a function of the external glucose concentration in a range between 3 mM and 12 mM, spanning physiological conditions from fasting (low insulin, high glucagon) to feeding (high insulin, low glucagon) [8]. PPH are more responsive to changes in the plasma glucose levels; that is, PPH are more gluconeogenic at low glucose concentrations and become more glycolytic at high glucose concentrations. At physiological plasma concentrations of glucose in the range of 6–8 mM, PCH are more glycolytic than PPH. Importantly, the set point (i.e., the external glucose concentration at which the hepatocyte switches from glucose production to glucose consumption) shifts from 6.5 mM for PCH to 8 mM for PPH.

The capacity of PPH and PCH to metabolize glycerol and the two important food-derived monosaccharides fructose and galactose is depicted in Fig. 3C–E. While there is no zonal difference in the glycerol uptake rate, PPH have a higher capacity to metabolize fructose and galactose than PCH. Fig. 3F shows that the ability to store glycogen is equal in the two zones.

Zonation of fatty acid metabolism

Zone-dependent differences in the metabolism of fatty acids were examined by computing the cellular uptake rate of free fatty acids (FFAs) and the rate of central pathways of lipid metabolism in dependence of external FFA concentrations (Fig. 4). Up to external concentrations of FFAs of ~0.8 mM, the uptake rate of FFAs is independent of the zonal localization of the hepatocyte. At higher plasma concentrations, the uptake rate of PCH reaches saturation, while the uptake capacity of PPH does not. The same saturation kinetics in the load characteristics for PCH are observed in the synthesis rate of TAG, the size of the TAG pool and the synthesis rate of VLDL, which, however,

differ only marginally in PPH and PCH at lower concentrations of FFAs. A stronger response of PCH to variations of external concentrations of FFAs is predicted for the β-oxidation of FFAs and the synthesis of ketone bodies.

The hepatic uptake of glucose and FFAs is counter-regulated. At low plasma glucose levels, the liver operates as a glucose producer, and lipolysis in adipose tissue increases the plasma level of FFAs and promotes their uptake into hepatocytes. At high plasma glucose levels, the liver operates as a glucose consumer, and the high insulin level promotes the uptake and esterification of FFAs in adipose tissue. This inverse relationship between the plasma glucose level and FFA uptake is reflected in the load characteristics shown in Fig. 4G. The load characteristics indicate that for glucose concentrations above 4 mM, PPH and PCH do not differ in the glucose-dependent uptake of FFAs. However, clear differences exist in the glucose-dependency of FFA-utilizing pathways such as the synthesis of cholesterol, FFAs and VLDL. Generally, PPH appear to possess a higher lipid synthesizing capacity than PCH. This is also reflected in a higher share of *de novo* synthesized TAG (DNL) in the total cellular TAG pool.

Zonal differences in detoxification capacities

Clearance of potentially harmful metabolites from the blood is one of the most important liver functions. We analyzed the capability of PPH and PCH to extract ammonia and ethanol from the plasma. In the liver, ammonia can be fixed in the form of either urea or glutamine. The urea cycle catalyzes irreversible ammonia fixation, whereas ammonia fixation by glutamine synthesis is reversible, as ammonia can be liberated from glutamine by glutaminases. Fig. 5A–C depicts the rates of ammonia uptake, urea production and glutamine synthesis in PPH and PCH at varying external ammonia concentrations. Averaged across the six animals, the ammonia uptake is about four times higher in PPH and the metabolic fate of ammonia is completely different in the two cell fractions. While PPH fix the ammonia almost exclusively in the form of urea, PCH have a very high rate of glutamine synthesis. No zone-dependent differences were obtained for ethanol detoxification.

Zonal differences in energy metabolism

As PPH and PCH exhibit differences in central energy delivery and energy consumption pathways of carbohydrate, fatty acid and ammonia metabolism, it seems obvious that there are also zonal differences in the energetic state of the two cell fractions. We thus analyzed the energetic state (measured by the adenylate charge and the ATP/ADP ratio), the rate of gluconeogenesis, the rate of

ammonia detoxification and the rate of TAG synthesis in response to varying oxygen concentrations (Fig. 6A-H). Our computations predict a significantly lower ATP/ADP ratio and adenylate charge of PCH than of PPH. Gluconeogenesis of PCH is also more sensitive to falling oxygen pressure. Generally, all metabolic functions become independent of oxygen pressure at pO_2 > 25 mmHg due to oxygen saturation of complex IV of the respiratory chain.

Discussion

Metabolic zonation: The quantitative view

The aim of our work was to unravel the functional implications of the heterogeneous allocation of protein mass to the central metabolism of hepatocytes residing in the portal and central regions of the acinus. Numerous papers have already reported on the zonation of metabolic enzymes revealed at the transcriptional and translational levels of gene expression or by directly assaying enzyme activities. However, inferring from such data the flux changes of the related metabolic pathways is problematic in view of the enzyme-regulatory mechanisms operating after gene expression [16]. Therefore, we have chosen an approach that combines experimentally determined protein abundances in zone-specific cell fractions with a kinetic model of hepatocyte metabolism that has been extensively validated based on metabolic experiments with hepatocytes, liver tissue and perfused livers. This approach enabled us to overcome the conventional, ontology-based classification of zone-dependent pathway capacities into “higher or lower or equal” by a quantitative assessment of cell functions in response to typical changes of the blood plasma.

Isolation of periportal and pericentral hepatocytes by flow cytometry

During the past two decades, successful attempts to isolate pure hepatocyte populations from whole liver by flow cytometry have been made [17–20], overcoming hurdles such as the vast hepatocyte size and intense autofluorescence. However, up to now, flow cytometry has been used predominantly for the isolation and study of hepatocyte populations derived from the whole liver, and early attempts at the acinar zone-specific isolation of hepatocytes by cell sorting did not prevail [21]. More recently, imaging techniques such as immunohistochemistry and *in situ* hybridization have been developed, enabling the isolation of cells based on the presence of specific marker proteins [22]. For the separation of hepatocytes from the PP and PC regions by flow cytometry, we exploited the fact that surface protein E-Cad. and the metabolic enzyme GLUL are strictly zonated in the mouse acinus [23,24]. The analysis of the proteomic data of our sorted cells confirms the classical

pericentral zonated proteins such as GLUL, OAT, Cyp7A1 as well as many proteins of drug metabolism (e.g. CYP2E1, CYP1A2 and CYP2C29) for which heterogeneous distribution has been known for many years [25,26]. The periportal fraction also contains the classical representatives, such as HAL, mitochondria proteins like SFXN1, COX7A1 [5,27] as well as HSD17B6 [28] and PIGR [29]. In addition, the analyses also show a clear zonation of proteins, that the heterogenic distribution of which along the liver acinus has not been known, such as LGASL1 as well as SHROOM in the PCH fraction. However, if looking at the functions of these proteins, it does not seem so unlikely that they are subject to a clear zonation. For example, the strongly zoned expression of galectin could also be confirmed by its function as an immune/inflammatory regulator which acts both extracellularly and intracellularly, modulating innate and adaptive immune responses [30]. In the last decade first evidence shows that many processes of innate immunity are also not homogeneously distributed in the liver. In this regard, MacParland and co-workers could show that the pericentral localized endothelial cells probably have the largest proportion of the innate immune response in the healthy liver [31]. Taken together this separation technique improved the specificity of isolated hepatocytes from the different zones compared to the commonly used digitonin-collagenase perfusion [32]. Proteomics-based determination of enzyme abundances in the separate cell fractions and usage of protein abundances in an advanced kinetic model of hepatocyte metabolism enabled us to make *in silico* predictions of the metabolic performance of PPH and PCH. The results obtained by our systems biology approach confirmed some already known features and revealed additional features underlying the “division of labor” [10] in liver metabolism.

Carbohydrate metabolism

Earlier studies on the zonation of carbohydrate metabolism in the liver have provided evidence that PPH and PCH differ in their gluconeogenic and glycolytic capacities [6,33]. However, the extent of these zone-dependent differences is now known to be highly dynamic, depending, for example, on nutritional state and circadian rhythms [34]. In concordance with results in [35], our data suggest that both populations of hepatocytes act as a “glucostat” [36], producing glucose when blood glucose levels are below a critical set point (fasting) and utilizing glucose when blood glucose levels are above the set point (e.g., after a meal) (see Fig. 3B). In agreement with literature data, our model computations suggest that PCH are more glycolytic than PPH. In PPH, the protein abundances of the lactate transporter, GLUT2 and PCJP, as well as key regulatory enzymes of gluconeogenesis, such as PEPCK, FBP2/PFK2 and GK, are higher than in PCH. In line with this, Ogawa et al. [37]

found a stronger expression of the insulin-independent but concentration-dependent glucose transporter GLUT2 in PPH.

Gluconeogenesis from lactate is reported to be more prominent in PPH [38]. This is confirmed by our computations suggesting a remarkably diminished gluconeogenic capacity of PCH (Fig. 3A). Our computations also suggest zone-dependent differences in the utilization of the two important food-derived monosaccharides, galactose and fructose (see Fig.3D–E). Several enzymes involved in the metabolism of these monosaccharides, such as aldolase B (portal:central abundance ratio R=2.48), triose kinase (R=1.88), GLUT2 (R=1.9), fructokinase (R=1.28) and the galactose transporter (R=1.9), have a higher abundance in cells within the PP region.

Lipid metabolism

Fatty acids formed *de novo* (DNL), by lipolysis of TAG stores in lipid droplets or taken up from the plasma, can be used to yield acetyl-CoA in the process of β-oxidation or can be esterified with glycerol to form TAG stored in lipid droplets or lipoproteins (VLDL). Our analysis revealed almost identical uptake rates of FFAs up to plasma concentrations of approximately 0.8 mM, which is higher than the values observed in C57Bl/6N mice under an oral fat load [39]. Thus, the observation that the accumulation of fat (steatosis) in adults starts preferentially in the PC region cannot be explained simply by differences in the capacity of PPH and PCH. It should be noted, however, that we have assessed the uptake rate of FFAs under conditions of very low external glucose concentrations also applied in related *in vitro* experiments.

Another source for hepatic fatty acids is DNL from cytosolic acetyl-CoA derived from citrate by the ATP-dependent citrate lyase. Our analysis suggests that PPH synthesize more FFAs and possess a higher fraction of newly synthesized TAG due to the higher abundance of fatty acid synthase (PP:PC R=1.4), acetyl-CoA carboxylase (R=1.2) and ATP citrate lyase (R=2.8) compared with PPH. The literature findings on the zonation of DNL are contradictory. Our results are in line with those of Evans et al. [40], who showed a preponderance of all three mentioned enzymes in the PPH. However, the majority of publications conclude that DNL is more pronounced in PCH [41]. It is important to note that the relative contribution of DNL to the total pool of cellular fatty acids depends strongly upon the external glucose concentration. A steep increase in DNL occurs at high external glucose concentrations when plasma concentrations of FFAs are low and the uptake rate of fatty acids is low in both PPH and PCH (Fig. 4J).

Regarding the synthesis and export of VLDL, our analysis predicts a strong increase with increasing concentrations of FFAs in concordance with previous findings [42–44]. The export capacity for VLDL of PPH exceeds that of PCH regardless of the fatty acid uptake rate (Fig. 4D). In particular, at low glucose, the VLDL release rate in PPH is significantly higher than in PCH. This model-based prediction is supported by the fact that some marker proteins involved in the assembly and secretion of VLDL particles are enriched in PPH, including microsomal triglyceride transfer protein (PP:PC R=1.24), protein disulfide-isomerase A (R=2.1) and vesicle-trafficking protein SEC22b (R=1.6).

Likewise, we found higher rates of cholesterol synthesis in PPH than in PCH (Fig. 4H). In agreement with this finding, Cheng et al. [43] also found a predominance of cholesterol synthesis in the PP zone. Moreover, Li et al. [45] and Singer et al. [46] reported that HMG-CoA-reductase, the main regulatory enzyme of cholesterol synthesis [11], is almost exclusively found in the first hepatocytes in the PP area. A higher capacity for cholesterol synthesis in PPH than in PCH fits well with the higher VLDL secretion rates, as cholesterol and cholesterol esters are major constituents of VLDL particles. The higher capacity of PPH than PCH to export TAG in terms of VLDL could also explain the disease pattern of early hepatic steatosis in adults, which is predominantly PC centered [41,47]. Understanding differences in the lipid metabolism of PPH and PCH *in vivo* also requires taking into account porto-central differences in the sinusoidal blood flow and plasma concentration of metabolites (in particular oxygen, glucose and FFAs) and hormones.

Ammonia metabolism

In addition to the zonal effects of carbohydrate metabolism, the ammonia detoxification is the best examined zonated liver function. The liver possesses two alternative pathways for ammonia detoxification which are strictly separated along the porto-central axis: conversion to urea or glutamine. This view is confirmed by our analysis. Interestingly, the total capacity for ammonia detoxification in the physiological range (plasma levels of ammonia <0.5 mM) is almost the same in the two zones (Fig. 5A). That is, despite large zonal differences in the capacity of the urea cycle and glutamine synthesis, significant porto-central differences in the total ammonia-detoxifying capacity are expected for external ammonia concentrations that lie far above the physiological value of approximately 80 µM in mice [48]. In the PP zone, ammonia detoxification is achieved almost exclusively by urea formation, whereas in the PC zone, glutamine synthesis accounts for almost all ammonia removal. The strict division of ammonia detoxification between the urea cycle and GLUL fits to with the work of Braeuning et al. [29], who found a complete lack of GLUL in the PP zone and

a preferential location (PP:PC abundance ratios of 1.5–1.77:1) of mRNAs of urea cycle enzymes (OTC, ASS, ASL, and ARG) in the PP area. We found protein abundance ratios of 0.84, 1.64 and 4.72 for the three enzymes. More importantly, CPS1, the main regulatory enzyme of the urea cycle, occurs with 2.76-fold higher abundance in the periportal zone than in the PC zone.

Energy metabolism

Hitherto, little was known about the zonal distribution of adenine nucleotides and energetic state between the PP and PC zones. The proteomics data point to an increased capacity of PPH, compared to PCH, to generate ATP via oxidative phosphorylation due to the increased abundance of some proteins of the respiratory chain, including complexes I-IV (R=1.2–2.2), F0F1-ATPase (R=1.76), ANT (R=1.73) and mitochondrial phosphate exchanger (R=1.53). The better endowment of PPH with proteins of oxidative phosphorylation does not necessarily imply a higher ATP level, as PPH also have a higher capacity for excessively ATP-demanding processes such as gluconeogenesis and urea synthesis than PCHs. Balancing the opposing facts against each other, the model computations suggest a higher adenylate charge as well as a higher ATP/ADP ratio in PPH than in PCH. This finding is in agreement with the portal-to-central declining ATP level measured in a millifluidic media perfusion system that enables cells to be cultured in a slow-flow environment. Closer inspection of the regulatory circuits entailing this energetic difference between PPH and PCH yields the following explanation: mutual regulation of fatty acid oxidation and aerobic glycolysis as the main source of ATP production proceeds via the NADH- and acetyl-CoA dependent inhibition of the PDHC reaction, the entry point of glucose-derived carbons into the citric acid cycle. At reduced rates of β-oxidation, rising NAD and CoA levels activate PDHC, rendering glycolytic pyruvate the prevailing energy-delivering substrate. The switch from fatty acids to glucose goes along with a falling mitochondrial redox state and a transient and moderate downregulation of the respiratory chain and ATP production rate that is subsequently compensated for by a kinetic upregulation of the RC as a consequence of the reduced ATP level. Therefore, the computed zonal differences in ATP levels reflect zonal differences in substrate preference rather than in the local energy demand of hepatocytes.

Ethanol metabolization

In the healthy liver, ethanol is predominantly degraded by ADH, converting ethanol to acetaldehyde and the ALDH converting acetaldehyde l to acetate. Zone-dependent expression differences with a

PP:PC R=1.6 for ADH has been reported by Salsano et al. [49], while our data yield R = 1.2 for ADH and R = 0.45–4.5 for mitochondrial ALDHs. Based on these zone-dependent expression differences, our model yielded only marginal differences in the ethanol detoxification capacities of PPH and PCH (Fig. 5D).

Metabolic capacities of the Intermediate zone

While the focus of our study was clearly on the elucidation of possible metabolic differences between the periportal and pericentral zone, we also analyzed the metabolic capacities of Ecad-negative and CS-negative cells stemming from the intermediate zone (preliminary data given in Table S6). These preliminary results suggest that the intermediate zone has comparable capacities for the uptake and release of glucose as the pericentral zone whereas the uptake capacities for fructose and galactose correspond to those of the periportal zone. The capacities for TAG synthesis and VLDL export were higher and the capacity for ß-oxidation was slightly lower than in in periportal and pericentral zone. Ammonia uptake and metabolization was comparable to the periportal zone, while ethanol detoxification was constant throughout all three zones. The capacities for the synthesis of fatty acid and cholesterol synthesis were just between those of the periportal and pericentral zone.

Concluding remarks

Our analysis showes that PPH and PCH exhibit significant differences in the protein abundance of approximately two-thirds of metabolic enzymes. These differences result from the fact that extracellular conditions, (e.g. nutrients and hormones), have a strong impact on gene expression which vary along the sinusoidal blood stream [9]. Our model-based analysis suggests that the functional differences implied by unequal enzyme abundances along the porto-central axis depend essentially on the actual plasma concentrations of metabolites and hormones. For example, despite large zonal differences in the capacity of the urea cycle and glutamine synthesis, significant porto-central differences in the total ammonia-detoxifying capacity are only expected for external ammonia concentrations that are far above the physiological value. Similarly, clear discrepancies in TAG synthesis and VLDL export are predicted to occur at FFAs concentrations above the physiological value of approximately 1 mM [50]. Generally, it appears that portal-to-central differences in liver metabolism become more pronounced if the plasma concentrations of glucose and free fatty acids start to deviate from their physiological values. It must be emphasized that this conclusion holds only

for short-time deviations where the liver's proteome does not adapt to a nutritional status that is different from the well-fed nutritional status of the mice in our study.

How variable gene expression will change the metabolic performance of PPH and PCH under diabetes, hyperammonia or dyslipidemia still remains to be addressed to gain a comprehensive mechanistic view of liver metabolism.

References

1. Mathew P, Thoppil D. Hypoglycemia 2019.
2. Holecek M. Evidence of a vicious cycle in glutamine synthesis and breakdown in pathogenesis of hepatic encephalopathy-therapeutic perspectives. Metabolic brain disease 2014;29:9–17.
3. Schliess F, Hoehme S, Henkel SG, Ghallab A, Driesch D, Böttger J, et al. Integrated metabolic spatial-temporal model for the prediction of ammonia detoxification during liver damage and regeneration. Hepatology (Baltimore, Md.) 2014;60:2040–2051.
4. Kietzmann T. Metabolic zonation of the liver: The oxygen gradient revisited. Redox Biology 2017;11:622–630.
5. Gebhardt R, Matz-Soja M. Liver zonation: Novel aspects of its regulation and its impact on homeostasis. World journal of gastroenterology 2014;20:8491–8504.
6. Jungermann K. Functional significance of hepatocyte heterogeneity for glycolysis and gluconeogenesis. Pharmacology Biochemistry and Behavior 1983;18:409–414.
7. Kang YB, Eo J, Mert S, Yarmush ML, Usta OB. Metabolic Patterning on a Chip: Towards in vitro Liver Zonation of Primary Rat and Human Hepatocytes. Scientific Reports;8:8951.
8. Tomlinson L, Hyndman L, Firman JW, Bentley R, Kyffin JA, Webb SD, et al. In vitro Liver Zonation of Primary Rat Hepatocytes. Front. Bioeng. Biotechnol. 2019;7:17.
9. Berndt N, Holzhütter H-G. Dynamic Metabolic Zonation of the Hepatic Glucose Metabolism Is Accomplished by Sinusoidal Plasma Gradients of Nutrients and Hormones. Frontiers in physiology 2018;9:1786.
10. Halpern KB, Shenhav R, Matcovitch-Natan O, Tóth B, Lemze D, Golan M, et al. Single-cell spatial reconstruction reveals global division of labour in the mammalian liver. Nature 2017;542:352.

11. Berndt N, Bulik S, Wallach I, Wünsch T, König M, Stockmann M, et al. HEPATOKIN1 is a biochemistry-based model of liver metabolism for applications in medicine and pharmacology. Nature communications 2018;9:2386.
12. Gebhardt R, Hengstler JG, Muller D, Glockner R, Buenning P, Laube B, et al. New hepatocyte in vitro systems for drug metabolism: metabolic capacity and recommendations for application in basic research and drug development, standard operation procedures. Drug metabolism reviews 2003;35:145–213.
13. Matz-Soja M, Aleithe S, Marbach E, Böttger J, Arnold K, Schmidt-Heck W, et al. Hepatic Hedgehog signaling contributes to the regulation of IGF1 and IGFBP1 serum levels. Cell communication and signaling : CCS 2014;12:11.
14. Burke ZD, Reed KR, Phesse TJ, Sansom OJ, Clarke AR, Tosh D. Liver Zonation Occurs Through a β-Catenin–Dependent, c-Myc–Independent Mechanism. Gastroenterology 2009;136:2316-2324.e3.
15. Gaasbeek Janzen JW, Gebhardt R, Voorde GH ten, Lamers WH, Charles R, Moorman AF. Heterogeneous distribution of glutamine synthetase during rat liver development. The journal of histochemistry and cytochemistry : official journal of the Histochemistry Society 1987;35:49–54.
16. Bulik S, Holzhütter H-G, Berndt N. The relative importance of kinetic mechanisms and variable enzyme abundances for the regulation of hepatic glucose metabolism—insights from mathematical modeling. BMC biology 2016;14:15.
17. Black KA, Novicki DL, Vincent JL, Smith GJ. Flow cytometric analysis of xenobiotic metabolism activity in isolated rat hepatocytes. Cytometry 1993;14:334–338.
18. Severgnini M, Sherman J, Sehgal A, Jayaprakash NK, Aubin J, Wang G, et al. A rapid two-step method for isolation of functional primary mouse hepatocytes: cell characterization and asialoglycoprotein receptor based assay development. Cytotechnology 2011;64:187–195.
19. Wyman J, Guertin F, Mansour S, Fournier M, Laliberté S. Use of mouse hepatocytes for the flow cytometric determination of DNA levels of nuclei extracted from fresh tissue of hybrid larch (Larix x eurolepis Henry). Cytometry 1993;14:217–222.
20. Gonçalves LA, Vigário AM, Penha-Gonçalves C. Improved isolation of murine hepatocytes for in vitro malaria liver stage studies. Malaria journal 2007;6:169.
21. Thalhammer T, Gessl A, Braakman I, Graf J. Separation of hepatocytes of different acinar zones by flow cytometry. Cytometry 1989;10:772–778.

22. Haroon MF, Skennerton CT, Steen JA, Lachner N, Hugenholtz P, Tyson GW. In-solution fluorescence in situ hybridization and fluorescence-activated cell sorting for single cell and population genome recovery. Methods in enzymology 2013;531:3–19.
23. Gebhardt R, Mecke D. Heterogeneous distribution of glutamine synthetase among rat liver parenchymal cells in situ and in primary culture. The EMBO journal 1983;2:567–570.
24. Doi Y, Tamura S, Nammo T, Fukui K, Kiso S, Nagafuchi A. Development of complementary expression patterns of E- and N-cadherin in the mouse liver. Hepatology Research 2007;37:230–237.
25. Monga SPS, ed. Molecular Pathology of Liver Diseases. Boston, MA: Springer Science+Business Media LLC, 2011.
26. Ben-Moshe S, Shapira Y, Moor AE, Manco R, Veg T, Bahar Halpern K, et al. Spatial sorting enables comprehensive characterization of liver zonation. Nature metabolism 2019;1:899–911.
27. Rönn T, Poulsen P, Hansson O, Holmkvist J, Almgren P, Nilsson P, et al. Age influences DNA methylation and gene expression of COX7A1 in human skeletal muscle. Diabetologia 2008;51:1159.
28. Cheng X, Kim SY, Okamoto H, Xin Y, Yancopoulos GD, Murphy AJ, et al. Glucagon contributes to liver zonation. Proceedings of the National Academy of Sciences of the United States of America 2018;115:E4111-E4119.
29. Braeuning A, Ittrich C, Kohle C, Hailfinger S, Bonin M, Buchmann A, et al. Differential gene expression in periportal and perivenous mouse hepatocytes. The FEBS journal 2006;273:5051–5061.
30. Potikha T, Ella E, Cerliani JP, Mizrahi L, Pappo O, Rabinovich GA, et al. Galectin-1 is essential for efficient liver regeneration following hepatectomy. Oncotarget 2016;7:31738–31754.
31. MacParland SA, Liu JC, Ma X-Z, Innes BT, Bartczak AM, Gage BK, et al. Single cell RNA sequencing of human liver reveals distinct intrahepatic macrophage populations. Nature communications 2018;9:4383.
32. Strain AJ. Isolated hepatocytes: use in experimental and clinical hepatology. Gut 1994;35:433–436.
33. Guder WG, Schmidt U. Liver cell heterogeneity. The distribution of pyruvate kinase and phosphoenolpyruvate carboxykinase (GTP) in the liver lobule of fed and starved rats. Hoppe Seylers Z Physiol Chem 1976;357:1793–1800.

34. Froy O. The relationship between nutrition and circadian rhythms in mammals. Frontiers in neuroendocrinology 2007;28:61–71.
35. Berndt N, Horger MS, Bulik S, Holzhütter H-G. A multiscale modelling approach to assess the impact of metabolic zonation and microperfusion on the hepatic carbohydrate metabolism. PLoS computational biology 2018;14:e1006005.
36. Jungermann K. Metabolische Zonierung des Leberparenchyms. Bedeutung für die Regulation des Glucostaten Leber. Die Naturwissenschaften 1985;72:76–84.
37. Ogawa A, Kurita K, Ikezawa Y, Igarashi M, Kuzumaki T, Daimon M, et al. Functional localization of glucose transporter 2 in rat liver. The journal of histochemistry and cytochemistry : official journal of the Histochemistry Society 1996;44:1231–1236.
38. Bracht A, Constantin J, Ishii-Iwamoto EL, Suzuki-Kemmelmeier F. Zonation of gluconeogenesis from lactate and pyruvate in the rat liver studied by means of anterograde and retrograde bivascular perfusion. Biochim Biophys Acta 1994;1199:298–304.
39. Yeh MM, Brunt EM. Pathological features of fatty liver disease. Gastroenterology 2014;147:754–764.
40. Evans JL, Quistorff B, Witters LA. Zonation of hepatic lipogenic enzymes identified by dual-digitonin-pulse perfusion. The Biochemical journal 1989;259:821–829.
41. Schleicher J, Tokarski C, Marbach E, Matz-Soja M, Zellmer S, Gebhardt R, et al. Zonation of hepatic fatty acid metabolism - The diversity of its regulation and the benefit of modeling. Biochim Biophys Acta 2015;1851:641–656.
42. Aarsland A, Wolfe RR. Hepatic secretion of VLDL fatty acids during stimulated lipogenesis in men. Journal of lipid research 1998;39:1280–1286.
43. Cheng HC, Yang CM, Shiao MS. Zonation of cholesterol and glycerolipid synthesis in regenerating rat livers. Hepatology 1993;17:280–286.
44. Franke H, Potratz I, Dargel R. Zonal differences in lipoprotein formation in the thioacetamide-induced micronodular-cirrhotic rat liver. Experimental and toxicologic pathology : official journal of the Gesellschaft fur Toxikologische Pathologie 1994;46:503–511.
45. Li AC, Tanaka RD, Callaway K, Fogelman AM, Edwards PA. Localization of 3-hydroxy-3-methylglutaryl CoA reductase and 3-hydroxy-3-methylglutaryl CoA synthase in the rat liver and intestine is affected by cholestyramine and mevinolin. Journal of lipid research 1988;29:781–796.
46. Singer II, Kawka DW, Kazazis DM, Alberts AW, Chen JS, Huff JW, et al. Hydroxymethylglutaryl-coenzyme A reductase-containing hepatocytes are distributed periportally in normal and

mevinolin-treated rat livers. Proceedings of the National Academy of Sciences of the United States of America 1984;81:5556–5560.
47. Takahashi Y, Fukusato T. Histopathology of nonalcoholic fatty liver disease/nonalcoholic steatohepatitis. World journal of gastroenterology 2014;20:15539–15548.
48. Koizumi T, Hayakawa J, Nikaido H. Blood ammonia concentration in mice: normal reference values and changes during growth. Laboratory animal science 1990;40:308–311.
49. Salsano F, Maly IP, Sasse D. The circadian rhythm of intra-acinar profiles of alcohol dehydrogenase activity in rat liver: a microquantitative study. The Histochemical journal 1990;22:395–400.
50. Fernandez J, Valdeolmillos M. Increased levels of free fatty acids in fasted mice stimulate in vivo beta-cell electrical activity. Diabetes 1998;47:1707–1712.

Tables:

Table 1: Mean Label Free Quantification (LFQ) of most potent zonated proteins

Figure Legends:

Fig. 1: Schematic model representation

Reactions and transport processes between compartments are symbolized by arrows. Single pathways as defined in biochemical text books are numbered and highlighted by different coloring: (1) glycogen metabolism, (2) fructose metabolism, (3) galactose metabolism, (4) glycolysis, (5) gluconeogenesis, (6) oxidative pentose phosphate pathway, (7) non-oxidative pentose phosphate pathway, (8) fatty acid synthesis, (9) triglyceride synthesis, (10) synthesis and degradation of lipid droplets and synthesis of VLDL lipoprotein, (11) cholesterol synthesis, (12) tricarbonic acid (TCA) cycle, (13) respiratory chain & oxidative phosphorylation, (14) β-oxidation of fatty acids, (15) urea cycle, (16) ethanol metabolism, (17) ketone body synthesis, (18) ammonia formation, (19) serine utilization, (20) alanine utilization. Small cylinders and cubes symbolize ion channels and ion transporters. Double-arrows indicate reversible reactions, which may proceeded in both directions according to the value of the thermodynamic equilibrium constant and cellular concentrations of their reactants. Reactions are labeled by the short names of the catalyzing enzyme or membrane transporter given in the small boxes attached to the reactions arrow. Red boxes indicate enzymes that are regulated by hormone-dependent reversible phosphorylation. Metabolites are denoted by their short names. Full names of metabolites and kinetic rate laws of reaction rates are outlined in

Berndt et al. [13].

Fig. 2: Sorting of pericentral and periportal hepatocytes via flow cytometry.
A: Immunofluorescence double staining shows distinct PP (E-Cadherin-magenta) or pc (GLUL-green) location along the porto-central axis. **B:** Fold change heatmap of the 39 strongest zonated proteins. Red boxes indicate out of range values (higher than 15-fold expression). The fold change of PPH and PCH cell populations to each other was calculated with the normalized LFQ intensities from the proteomic analysis. **C:** Western blot analysis of zone-specific markers in lysates from sorted GLUL positive (PCH) (N=3) and E-Cadherin positive (PPH) (N=3) hepatocytes. **D:** Western blot protein quantification normalized to total protein. Unpaired t test, *p ≤0.05

Fig. 3: Differences in hepatic carbohydrate metabolism of periportal and pericientral hepatocytes.
Red: Periportal hepatocyte (PPH); Blue: Pericentral hepatocyte (PCH); The solid lines represent the mean of six animals, the shaded areas indicate the standard deviations. The external conditions for each load characterisitics are given in Supplement 6.
A Rate of gluconeogenesis in dependence of plasma lactate concentration
B Glucose exchange flux in dependence of plasma glucose concentration
C Glycerol uptake flux in dependence of plasma glycerol concentrations
D Fructose uptake flux in dependence of plasma fructose concentration
E Galactose uptake flux in dependence of plasma galactose concentration
F Glycogen content in dependence of plasma glucose concentration

Fig. 4: Functional differences in hepatic fatty acid metabolism of periportal and pericientral hepatocytes.
Red: Periportal hepatocyte; Blue: Pericentral hepatocyte. Solid lines represent the mean of six animals and shaded areas depict standard deviations. See supplement 6 for the external concentrations of hormones and exchangable metabolites used for the computation of the load characteristics.
A Fatty acid uptake rate in dependence of plasma fatty acid concentrations

B Rate of TAG synthesis in dependence of fatty acid uptake rate
C Rate of TAG content in dependence of fatty acid uptake rate
D Rate of VLDL export in dependence of fatty acid uptake rate
E Rate of ketone body production in dependence of fatty acid uptake rate
F Rate of β-oxidation in dependence of fatty acid uptake rate
G Rate of fatty acid uptake in dependence of plasma glucose concentrations
H Rate of cholesterol synthesis in dependence of plasma glucose concentration
I Rate of fatty acid synthesis in dependence of plasma glucose concentration
J Realtive share of *de novo* synthesized TAG (DNL) on total fatty acid utilization
K Rate of VLDL secretion in dependence of plasma glucose concentrations
L Rate of β-oxidation in dependence of plasma glucose concentrations

Fig. 5: Comparison of ammonia and ethanol detoxification in periportal and pericientral hepatocytes.

Red: Periportal hepatocyte; blue: pericentral hepatocyte; solid line represents mean of six animals and ahaded area depicts standatt deviaton

A Rate of ammonia uptake in dependence of plasma ammonia concentrations
B Rate of urea production in dependence of plasma ammonia concentrations
C Rate of glutamine synthesis in dependence of plasma ammonia concentrations
D Rate of ethanol uptake in dependence of plasma ethanol concentrations

Fig. 6: Metabolic functions of PPH and PCH in dependence of oxygen concentration

Red: Periportal hepatocyte; Blue: Pericentral hepatocyte; solid line represents mean of six animals and ahaded area depicts standatt deviaton

A Relative rate of oxygen consumption
B Relative rate of glucose production
C Adenylate charge $AC = \frac{ATP + 0.5\,ADP}{AMP + ADP + ATP}$
D ATP/ADP ratio
E Uptake rate of ammonia
F Rate uf urea production
G Rate of glutamine synthesis
H Rate of TAG synthesis

Author Contributions

N.B., HG.H. and M.MS substantial contributions to conception and design, E.K. R.G., J.E., F.O. and D.M. acquisition, analyses and interpretation of the data; F.O. revising the article critically for important intellectual content; N.B., HG.H. and M.MS. final approval of the version to be published.

Acknowledgment

We like to thank Katrin Jäger and Andreas Lösche from the Core Unit Fluorescence Technologie at the Leipzig University for technical guidance and establishing of the flow cytometry experiments. Furthermore, we would like to thank Prof. Rolf Gebhardt for his valuable comments and recommendations regarding the establishment of FACS analysis methods. Gratitude is also expressed for the excellent technical assistence of Doris Mahn and Vivien Teßmar. Further, we would like to thank Dr. Petra Hirrlinger from the Medizinisches Experimentelles Zentrum (Faculty of Medicine) for taking excellent care of the mice.

Tables

Table 1: Mean Label Free Quantification (LFQ) of most potent zonated proteins

Protein IDs	**Protein names**	**mean LFQ E-Cad** mouse 1-6	**mean LFQ GLUL** mouse 1-6
P16045	Galectin-1	0.00E+00	1.40E+07
Q69ZF3;B1AWI3	Non-lysosomal glucosylceramidase	0.00E+00	3.01E+06
A3KG44;Q8VC91;E9Q2Y3;Q7TSS3;O88522; A3KG40;A3KG41;A3KG38	NF-kappa-B essential modulator	0.00E+00	5.28E+06
A7TU71;A2ALU4	Protein Shroom2	0.00E+00	4.17E+06
A2A4A6;Q62077;G3UXP4;F6SLL0	Phosphoinositide phospholipase C;1-phosphatidylinositol 4,5-bisphosphate phosphodiesterase gamma-1	0.00E+00	6.03E+06
A0A0R4J094;Q3TC72	Fumarylacetoacetate hydrolase domain-containing protein 2A	0.00E+00	1.37E+07
S4R1X1;Q7TMQ7;D3Z101;D3Z0V8	WD repeat-containing protein 91	0.00E+00	1.49E+07
Q8C025;D6RCW3;D3Z6W4;D3YU39	Cholinephosphotransferase 1	0.00E+00	2.41E+07
Q64505	Cholesterol 7-alpha-monooxygenase	0.00E+00	1.69E+07
P43006;A2APL5;F6ZRK3;F7CAM6;A2AQI7	Excitatory amino acid transporter 2;Amino acid transporter	0.00E+00	9.49E+07
P29758	Ornithine aminotransferase, mitochondrial	2.53E+07	6.29E+09
Q91X75;P20852;P15392;F7B9W9;F6SHL3; E9Q593	Cytochrome P450 2A5;Cytochrome P450 2A4	9.41E+06	1.33E+09
P15105;D3YVK1;D3Z121	Glutamine synthetase	3.60E+08	3.13E+10
P56654	Cytochrome P450 2C37	2.33E+07	9.19E+08
A2A977;O88833;A2A8T1;F8WGU9;A2A8S9; Q91WU1;A2A8S8	Cytochrome P450 4A10	8.75E+06	2.34E+08
O35728;A0A087WS15	Cytochrome P450 4A14	1.03E+07	1.97E+08
Q64458;Q3UT49;H3BLM0	Cytochrome P450 2C29	2.04E+08	3.28E+09
A2AVR6;Q8VHQ9;F6SS52;E0CYS0; E0CYA0;E0CXP8	Acyl-coenzyme A thioesterase 11	5.23E+05	7.76E+06
A0A1B0GSD0;Q9CRB3;A0A1B0GR99; A0A0A0MQC3	5-hydroxyisourate hydrolase	1.29E+07	1.78E+08
Q91X77	Cytochrome P450 2C50	3.73E+08	4.58E+09
P62874;H3BKR2;H3BLF7;Q61011	Guanine nucleotide-binding protein G(I)/G(S)/G(T) subunit beta-1	1.16E+06	1.34E+07
Q05421;A0A1B0GSV7;Q0PGA1	Cytochrome P450 2E1	2.63E+08	3.03E+09
O70572;D6RGM4	Sphingomyelin phosphodiesterase 2	9.86E+05	1.12E+07

Q9WVM8;Q3UNS8	Kynurenine/alpha-aminoadipate aminotransferase, mitochondrial	7.50E+06	8.36E+07
P00186	Cytochrome P450 1A2	3.82E+08	4.25E+09
Q6XVG2	Cytochrome P450 2C54	7.58E+07	8.35E+08
A2ASZ8;Z4YLR9;A0A0A6YWC1;F6RC04	Calcium-binding mitochondrial carrier protein SCaMC-2	1.28E+07	1.26E+06
A0A0A6YVS2;Q921L3	Transmembrane and coiled-coil domain-containing protein 1	3.94E+07	3.85E+06
P33267;A0A0U1RPL9	Cytochrome P450 2F2	3.10E+09	2.39E+08
Q64685	Beta-galactoside alpha-2,6-sialyltransferase 1	7.43E+06	5.39E+05
Q99JR1	Sideroflexin-1	7.85E+08	5.69E+07
P31649;D3YWZ5	Sodium- and chloride-dependent GABA transporter 2	1.95E+07	1.04E+06
P35492;F8WH73	Histidine ammonia-lyase	1.13E+09	4.20E+07
Q9R092	17-beta-hydroxysteroid dehydrogenase type 6	1.04E+08	2.28E+06
O70570;D3YVM4;D3Z2D3	Polymeric immunoglobulin receptor;Secretory component	6.31E+07	6.15E+05
E9QJY0;P18581	Cationic amino acid transporter 2	6.82E+06	0.00E+00
A0A140LIU4;P56392	Cytochrome c oxidase subunit 7A1, mitochondrial	1.31E+07	0.00E+00
A0A0R4IZW5;P09803	Cadherin-1;E-Cad/CTF1;E-Cad/CTF2;E-Cad/CTF3	1.78E+07	0.00E+00

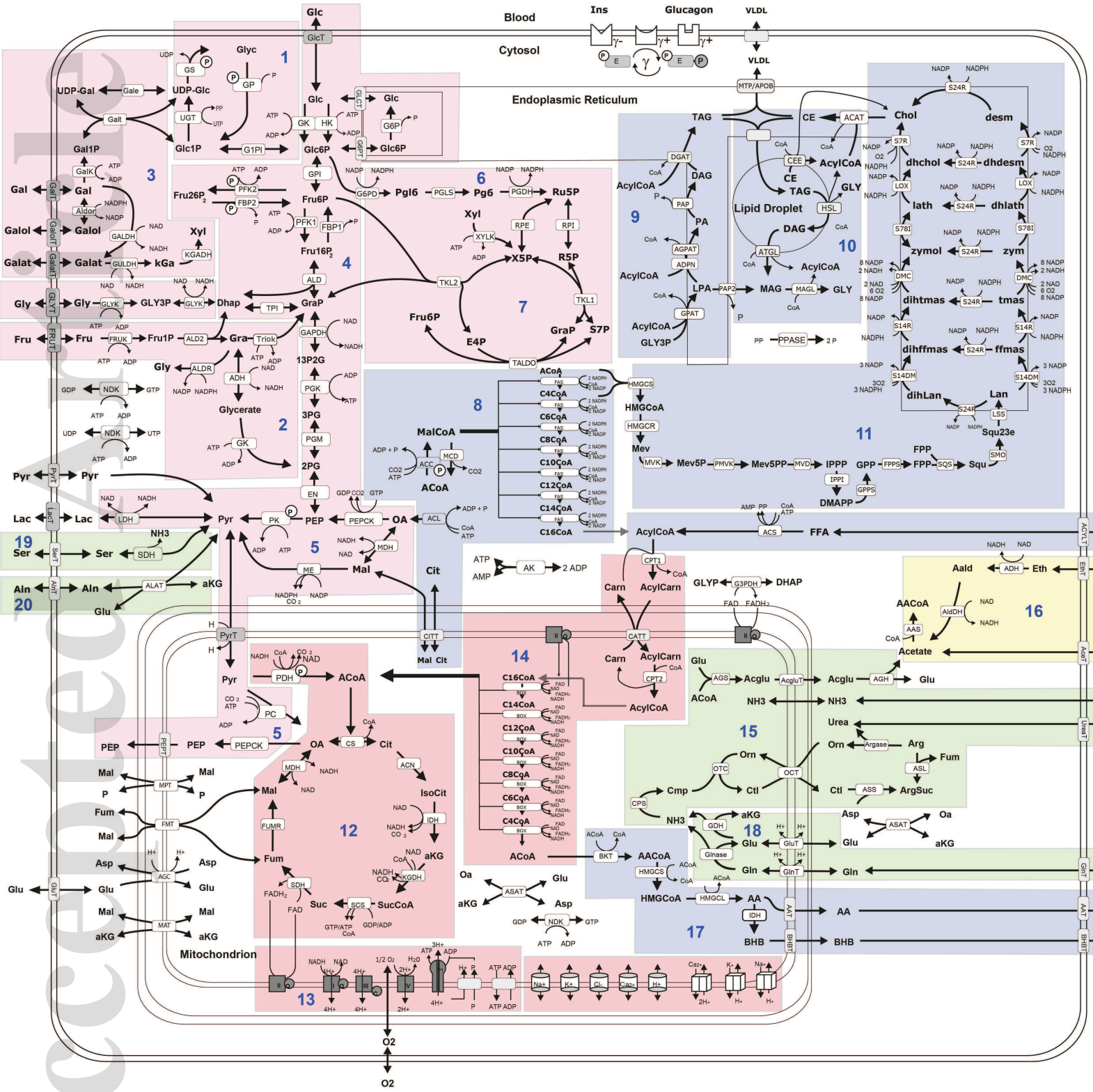

hep_31274_f1.eps

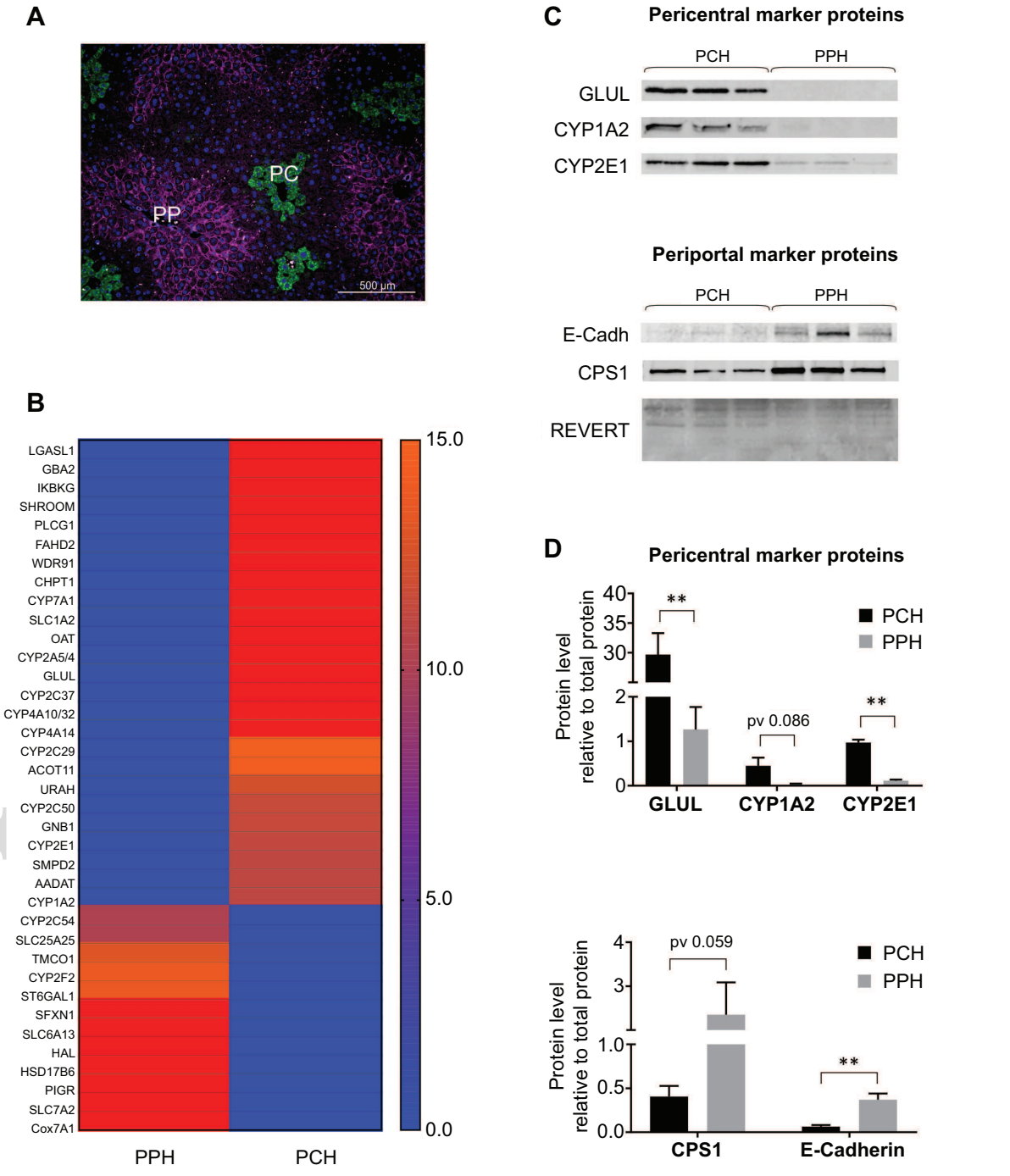

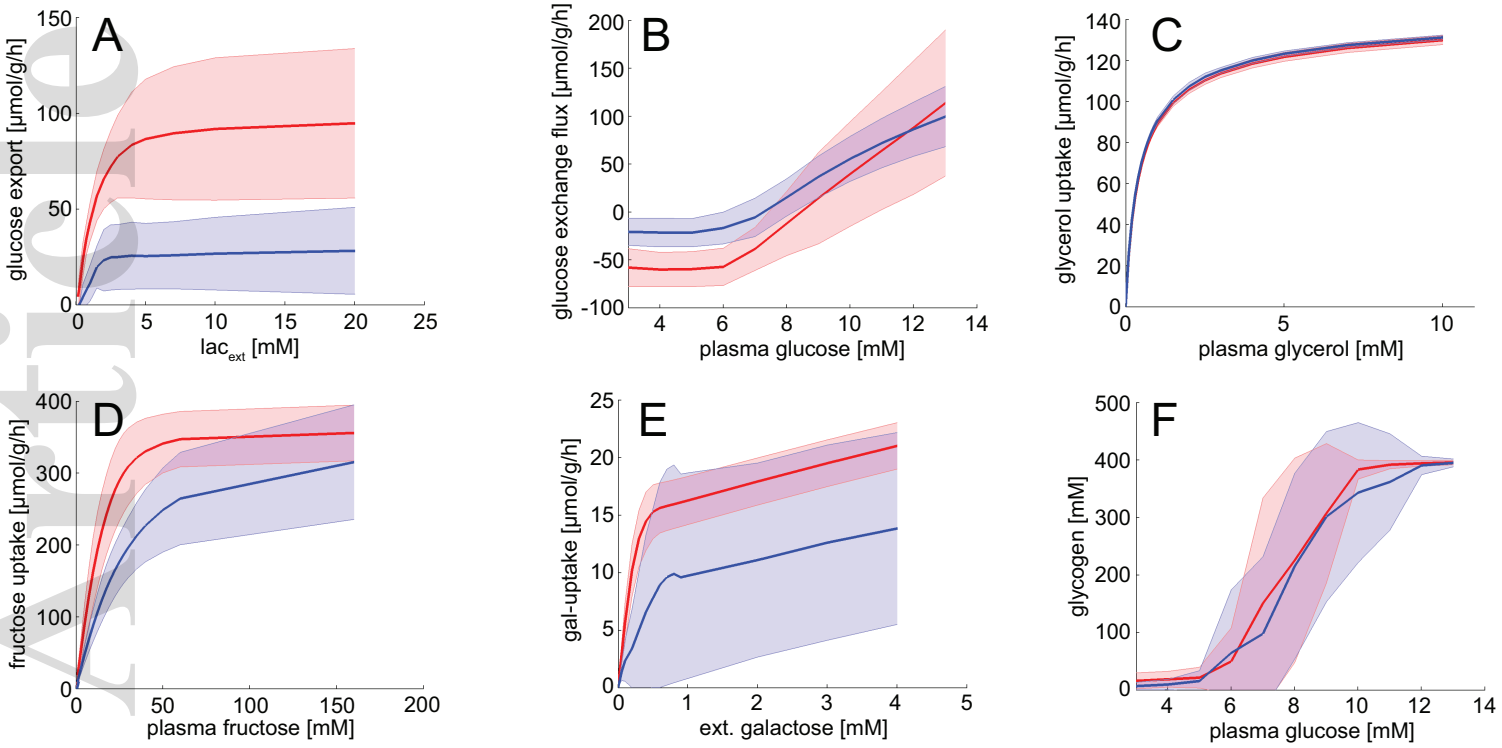

hep_31274_f3.eps

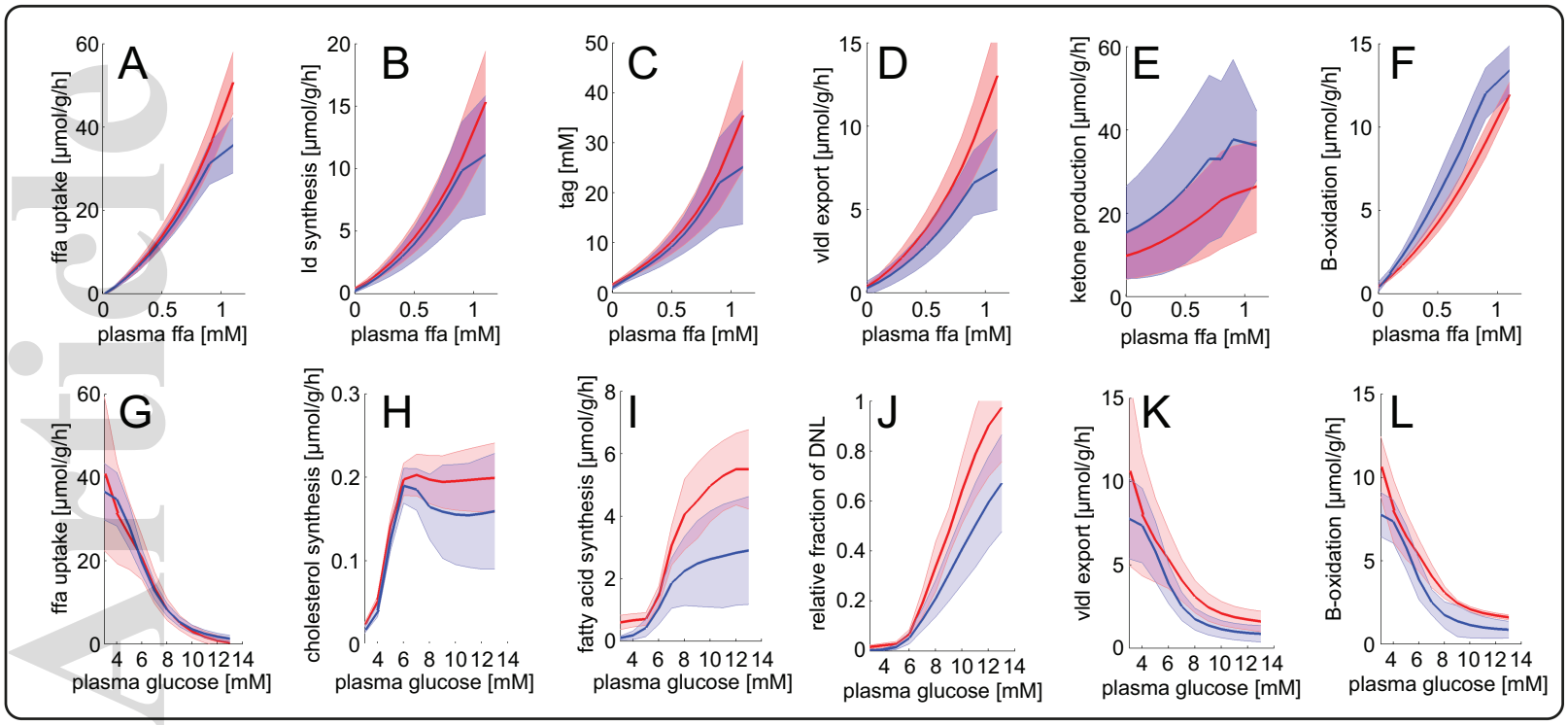

hep_31274_f4.eps

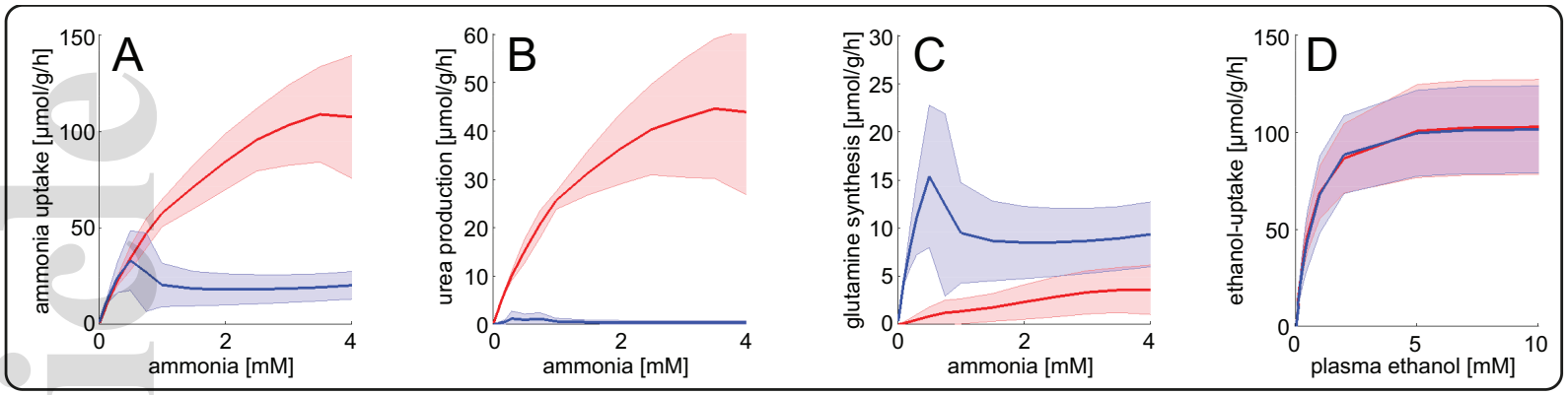

hep_31274_f5.eps

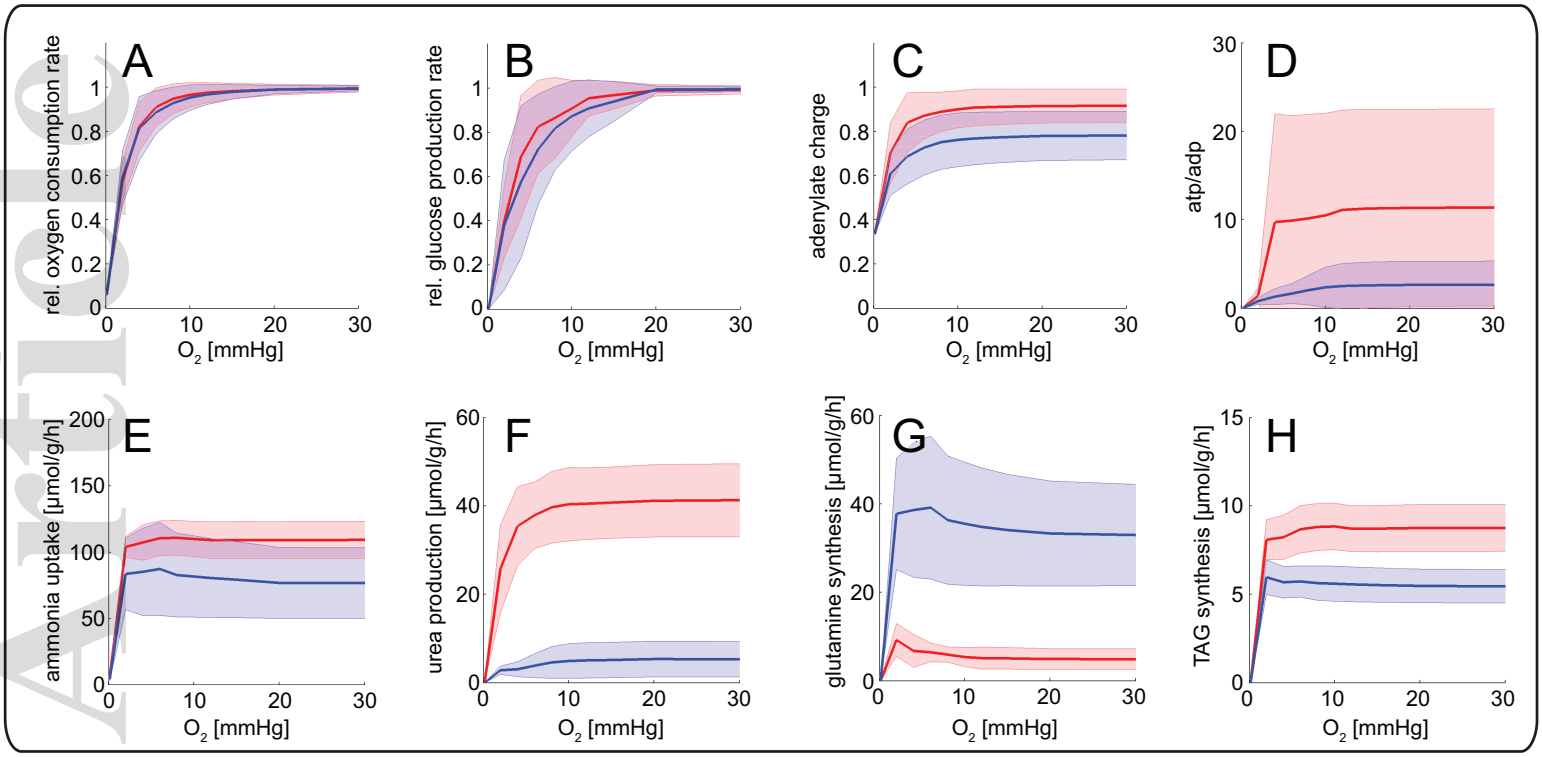

hep_31274_f6.eps